Measurement of the Intensity-Dependent Atomic Dipole Phase of a High Harmonic by Frequency-Resolved Optical Gating

Taro Sekikawa, Tomotaka Katsura, Satoshi Miura, and Shuntaro Watanabe

Institute for Solid State Physics, University of Tokyo, 5-1-5 Kashiwanoha, Kashiwa 277-8581, Japan

(Received 5 September 2001; published 26 April 2002)

The temporal profile and phase of the fifth harmonic of a Ti:sapphire laser were fully characterized by two-photon ionization frequency-resolved optical gating technique for the first time. The fifth harmonic was found to have negative chirp and the pulse compression was demonstrated. The negative chirp is well explained by using a zero-range potential model. This technique is scalable to extreme ultraviolet (XUV) and soft x-ray regions by using currently available light sources, making it possible to measure the pulse duration and phase of vacuum ultraviolet, XUV, and soft x-ray pulses.

DOI: 10.1103/PhysRevLett.88.193902 PACS numbers: 42.65.Re, 32.80.Rm, 42.65.Ky

High harmonics generated by nonlinear interaction between the intense laser field and atoms are of great interest for the potential application to science and technology in vacuum ultraviolet (VUV), extreme ultraviolet (XUV), and soft x-ray regions. Recently, theoretical analyses and experiments in the strong field approximation (SFA) reveal that high harmonic pulses have an intensity-dependent phase, i.e., atomic dipole phase, and that it plays a predominant role in the macroscopic properties of a high harmonic such as spatial and temporal coherence, phase matching, and frequency chirp [1–8]. Especially, the atomic dipole phase plays an important role in the temporal properties, because it induces negative chirp in a high harmonic pulse. Thus, appropriate phase compensation compresses the high harmonic pulses to the attosecond regime [9]. For that purpose, full phase characterization is necessary to obtain the phase distortion of a high-harmonic pulse.

One of the techniques commonly used for characterizing the ultrashort pulses fully is frequency-resolved optical gating (FROG) [10]. It involves measuring the time-dependent spectrum of the autocorrelation or cross correlation (spectrogram) and solving the pulse retrieval problem mathematically. The nonlinear optical processes used so far, however, require bulk materials as nonlinear media, through which XUV and VUV pulses cannot propagate. Another nonlinear process is necessary for the pulse measurement in the VUV and XUV regions.

In this paper, we propose two-photon ionization (TPI) FROG for the full characterization of XUV and VUV pulses and demonstrate the intensity and phase measurement of the fifth harmonic pulses of a Ti:sapphire (TiS) laser for the first time. TPI FROG is free from phase matching and is scalable to XUV and soft x-ray pulses. Here we focus on the fifth harmonic to demonstrate the versatility of TPI FROG, because the phase manipulation is easier by using the transport dispersive materials and because the validity of the measurement can be checked. We are also interested in the nonlinear response of the atomic polarization under a high electric field of 6×10^{13} W/cm^2. In this work, the phase of the fifth harmonic was found to be negatively chirped and is discussed by using a zero-range potential (ZRP) model [11–13], which can explain high harmonic generation fairly well above the third harmonic and includes the so-called two-step model [13–15]. The predictions of the ZRP model generally agree with that of the SFA model widely used for the explanation of high-harmonic generation in the strong field limit [16].

The TPI photoelectron spectrum is shown to be equivalent to the spectral resolved SHG as follows: From the second order perturbation theory, the nonresonant photoelectron spectrum is represented as

$$I(\omega - I_p/\hbar) \sim \left| \int_{-\infty}^{\infty} E(t)^2 \exp(-i\omega t)\, dt \right|^2, \quad (1)$$

where $E(t)$ is the time-dependent electric field, I_p is the ionization potential of target gas, and ω is the optical frequency. When two ultrashort pulses with a time interval of τ are used for TPI, the photoelectron spectrogram is

$$I_{\mathrm{FROG}}(\omega - I_p/\hbar/\tau) \sim \left| \int_{-\infty}^{\infty} E(t)E(t-\tau) \exp(-i\omega t)\, dt \right|^2 + f(\omega - I_p/\hbar), \quad (2)$$

which is identical to the SHG FROG trace after the subtraction of a time-independent TPI spectrum $f(\omega - I_p/\hbar)$ by two individual beams. Thus, TPI FROG can be analyzed by the same way as SHG FROG.

Figure 1 shows the experimental setup for TPI FROG measurement. Two spatially divided TiS laser pulses were focused into the Xe gas jet placed at a position of 2.5 cm after the focus to generate the fifth harmonic (7.75 eV). The fifth harmonic was separated from the other harmonics and the fundamental by using two beam splitters [17,18], a CaF_2 filter, and a concave dielectric multilayer mirror with a radius of curvature 10 cm for the fifth harmonic. The reflected fundamental beam was reduced by 8 orders of magnitude, making it possible to eliminate any nonlinear effects related to the fundamental. The pulse energy, the pulse duration, and the peak intensity at the gas jet were 7 mJ, 40 fs, and 6.0×10^{13} W/cm^2, respectively, at

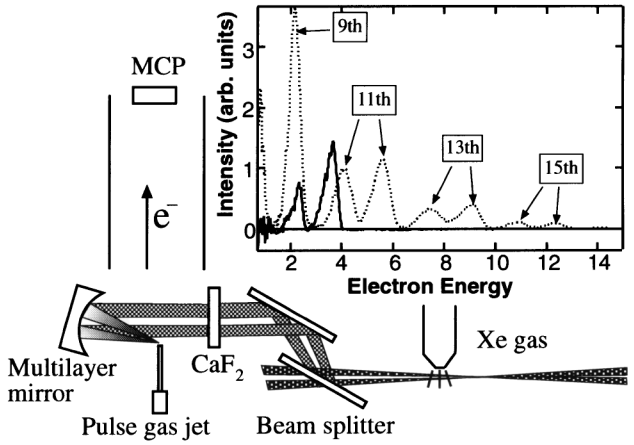

FIG. 1. Experimental setup for TPI FROG measurement. The inset shows the photoelectron spectra by high harmonics of a TiS laser (dotted line) and by the fifth harmonic (solid line).

a repetition rate of 10 Hz. CaF_2 plates with the thickness of 0.5, 2, and 4 mm were used to change the optical dispersion of the fifth harmonic. The generated two replicas of the fifth harmonic pulses were focused into the Xe gas jet for TPI. The ionization and the lowest excitation energies of Xe are 12.13 and 8.32 eV, respectively, which are well above one-photon energy and assure the nonresonant condition in the TPI process. The ejected photoelectrons were collected over $\sim 2\pi$ sr and detected by a microchannel plate (MCP) at each delay time after passing through a magnetic bottle electron spectrometer. The signals from MCP were recorded by a 8-Gs, 1-GHz digitizing oscilloscope and converted into a photoelectron spectrum by a computer to form a spectrogram.

The dotted line in the inset of Fig. 1 shows the photoelectron spectrum of Xe by the harmonics above the 7th taken by replacing the multiplayer mirror to an Al mirror and by removing a CaF_2 plate. Two peaks from the ground state of Xe, $^2P_{3/2}$ (12.13 eV) and $^2P_{1/2}$ (13.44 eV), were resolved at each harmonic order, and no other peaks by the mixing of the fundamental with harmonics were observed. The photoelectron spectrum shown by the solid line was obtained by the fifth harmonic with a CaF_2 plate and the multilayer mirror. The peaks appeared between the 9th and 11th, indicating TPI by the fifth harmonic. The photoelectron was retarded by applying an electric field to the time-of-flight tube to improve the spectral resolution of a TPI photoelectron spectrum to be better than 20 meV, which was good enough for TPI FROG. The spectral resolution was assured in comparison with the optical spectrum obtained by using a grating monochromator with a resolution of 2 meV. Special care was taken to avoid the spectral degradation due to the space-charge effect during experiment.

Figure 2 shows the 128×128 TPI FROG trace obtained with a 2-mm thick CaF_2 plate and the retrieved fifth harmonic pulse by the generalized projection algorithm [10]. This is the first full measurement of a high

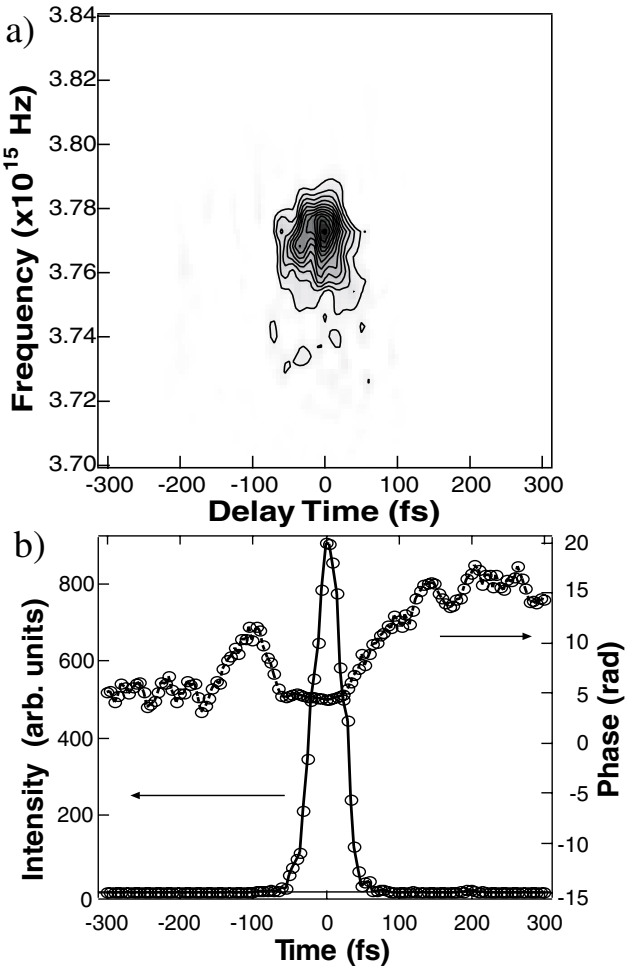

FIG. 2. (a) TPI FROG trace with the use of a 2-mm thick CaF_2 plate. (b) The solid and dotted lines are the intensity and phase profiles of the retrieved pulse, respectively.

harmonic pulse. The FROG error was 3%. Constant background by TPI and mean background of random noise were subtracted beforehand and super-Gaussian corner suppression and low-pass filters were applied for the optimal preparation of a TPI FROG trace. These techniques were shown to be effective for the pulse retrieval without introducing significant distortion [19]. We have checked the consistency of the retrieved pulse by comparing the frequency marginal with the observed spectrum [20].

The time direction of the retrieved pulse cannot be determined from one spectrogram, since TPI FROG utilizes the second order nonlinearity of the electric field. However, the direction can be determined by changing the thickness of the CaF_2 filter and by simulating the pulse shape, because a CaF_2 plate has positive dispersion at 160 nm. The solid lines in Fig. 3 show the retrieved pulses after the 0.5- and 4-mm plates. The dashed lines in Fig. 3 show the pulse shapes calculated from the pulse after a 2-mm thick CaF_2 plate by taking account of the dispersion relation of CaF_2. The calculated pulses are almost consistent with the retrieved pulses, indicating that the reuslts of TPI FROG

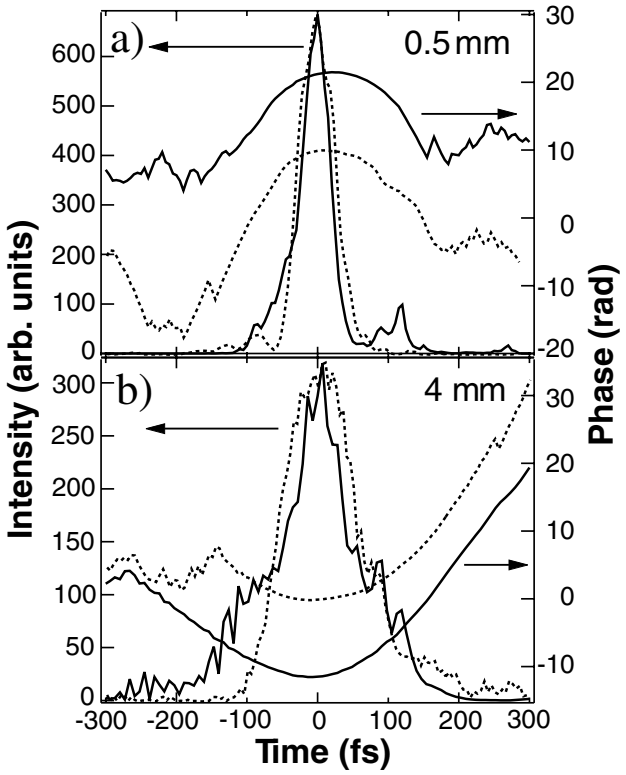

FIG. 3. Measured (solid lines) and calculated (dotted lines) pulse profiles and phases at the thickness of 0.5 (a) and 4 mm (b). The calculated pulse profiles are based on the pulse measured after the thickness of 2 mm of a CaF_2 plate. The phases are shifted vertically for clarification.

are reliable. Thus, the time direction of the retrieved pulse was determined as shown in Figs. 2 and 3. The pulses after 0.5- and 4-mm plates were found to have negative and positive chirp, respectively, and the frequency chirp was almost compensated around 2 mm. Then, the pulse without a CaF_2 plate can also be calculated and is shown in Fig. 4. The pulse duration was 80 fs. From the experimental results, the following two points were found. First, the generated harmonic pulse has negative chirp. The estimated quadratic coefficient of the phase before a CaF_2 plate is -5×10^{26} rad/sec^2. Second, the positive dispersive material compensates or overcompensates the phase: The phase with a 2-mm plate was almost constant around the pulse peak with a pulse duration of 50 fs, while the phases after 0.5- and 4-mm plates were parabolic.

Two origins of the negative chirp are considered: One is the phase modulation by ionization and the other is the atomic dipole response to the electric field. The creation of free electrons with the temporal evolution of a pulse induces the refractive index change within the pulse, resulting in the phase modulation. However, the peak intensity of the fundamental pulse is lower than the ionization threshold of Xe, which is approximately 1×10^{14} W/cm^2. Thus, it is concluded that the negative chirp of a high harmonic is due to the atomic dipole response. In the case of high harmonics with the photon

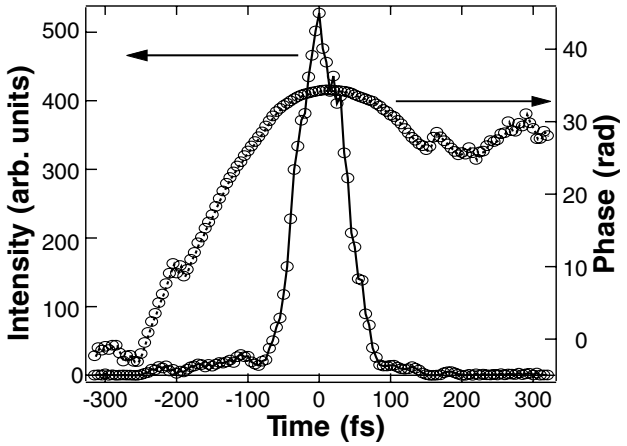

FIG. 4. Pulse shape just after generation calculated from the measured pulse after a 2-mm thick CaF_2 plate. The solid and dotted lines show the intensity and phase, respectively.

energies higher than the ionization energy under high laser intensity, the SFA model predicts the intensity-dependent atomic dipole phase [2]. However, lower harmonics are beyond the SFA model, and the phases of lower harmonics have never been investigated.

Now, we note that the ZRP model gives a harmonic spectrum similar to the numerical calculation of the time-dependent Schrödinger equation [13] above the third harmonic, when the binding energy of an electron is adjusted to the first excited state instead of the ionization potential. Both calculations agree quite well with the experimental results [21]. The ZRP model assumes a three-dimensional δ-function potential of an atom still retaining some features in common with a real atom, while the binding potential does not enter explicitly in the SFA model, which ignores the interaction process of an electron with the laser field before it returns to the ground state [16]. As a result, the former model includes effects of the atomic potential and explains the generation of relatively lower-order harmonics well. Of course, both models agree well with each other in the high intensity region. We have simulated the intensities and the phases of several high harmonics for both models and then found that the calculated results generally agree in the strong field limit. Thus, the ZRP model was used for the simulation of the fifth harmonic.

The fifth dipole moment was numerically calculated at various laser intensities by using the first excitation energy instead of the ionization potential [13]. Then the quantum-path analysis proposed by Balcou and co-workers was made to disentangle the intensity dependence of the phase [22,23]. In their analysis, the local slopes of the intensity dependence of the 45th harmonic phase were calculated and then are mapped on the intensity versus slope plot, showing two main quantum paths with slopes of $\alpha = 1.3 \times 10^{-14}$ and $\alpha = 25.5 \times 10^{-14}$ cm^2/W contributing high-harmonic generation clearly. In the case of the fifth harmonic, a strong component with a slope of

$\alpha = 5.9 \times 10^{-15}$ cm^2/W was found around an intensity of 6×10^{13} W/cm^2. This intensity-dependent phase indicates that the dipole moment of the fifth harmonic has negative chirp components. When the fundamental pulse with a Gaussian pulse shape $I(t)$ is approximated by a parabola, the intensity-dependent phase $\Phi(t) = \alpha I(t)$ is expressed as

$$\Phi(t) = \alpha I_0 \left(1 - \frac{4\ln(2)}{\tau_0^2} t^2\right), \tag{3}$$

where τ_0 and I_0 are the pulse duration and the peak intensity of the fundamental pulse, respectively. Therefore, the generated harmonics have negative parabolic phase when α is positive and can be compressed by optical components with the positive group velocity dispersion. By comparing the experimentally obtained quadratic coefficient with Eq. (3), the coefficient α is estimated to be 4.8×10^{-15} cm^2/W, which is in good agreement with the abovementioned simulation by the ZRP model. Consequently, the obtained slope is attributable to the strong component around zero in the quantum path analysis. Phase mismatch calculation including the Gouy phase and the obtained intensity-dependent atomic phase indicates that the phase mismatch is small when the gas jet is placed after the focus of laser, suggesting that the intensity-dependent phase with a small coefficient is selected by phase matching. The same phase matching and selection of the quantum path has also been discussed theoretically and experimentally in higher harmonics [3,8,24].

Finally, the TPI FROG is scalable for the characterization of the XUV and soft x-ray pulses generated by femtosecond lasers by the following three schemes: One is the scheme demonstrated in this paper, which is applicable up to the 13th harmonic of TiS laser pulses by changing rare gases. We have already demonstrated TPI of helium gas, of which TPI cross sections are approximately 10^{-51} cm^4 s [25], by the ninth harmonic pulses with a peak intensity of 115 GW/cm^2 [26]. Since the TPI cross section of helium gas is almost constant from the ninth to 13th harmonic [25], it is possible to characterize the high-harmonic pulses by TPI FROG. Another TPI scheme has been proposed by Schnürer *et al.* to observe nonlinear phenomena induced by high harmonics [27]. According to them, high-harmonic pulses at 13 nm generated by their state-of-the-art femtosecond laser are intense enough to cause the two-photon absorption from K shell to a free state in boron in spite of a small cross section at a shorter wavelength and the expected electron number is 10^4 sec^{-1}. By measuring the ejected photoelectron spectrum, TPI FROG should be feasible. The other scheme is the cross correlation between high harmonic and the fundamental pulse, which has been extensively applied to the temporal measurement of high harmonics so far [28–31]. FROG is applicable to the cross correlation scheme by using the principle component generalized projection algorithm [32] TPI FROG is a useful technique to evaluate high-harmonic pulses.

[1] M. Lewenstein *et al.,* Phys. Rev. A **49**, 2117 (1994).
[2] M. Lewenstein, P. Salières, and A. L'Huillier, Phys. Rev. A **52**, 4747 (1995).
[3] P. Salières, A. L'Huillier, and M. Lewenstein, Phys. Rev. Lett. **74**, 3776 (1995).
[4] M. Bellini *et al.,* Phys. Rev. Lett. **81**, 297 (1998).
[5] P. Salières *et al.,* Adv. At. Mol. Opt. Phys. **41**, 83 (1999).
[6] T. Sekikawa *et al.,* Phys. Rev. Lett. **83**, 2564 (1999).
[7] L. L. Déroff *et al.,* Phys. Rev. A **61**, 043802 (2000).
[8] P. Salières *et al.,* Science **292**, 902 (2001).
[9] P. Salières *et al.,* Phys. Rev. Lett. **81**, 5544 (1998).
[10] R. Trebino *et al.,* Rev. Sci. Instrum. **68**, 3277 (1997).
[11] W. Becker, S. Long, and J. K. McIver, Phys. Rev. A **41**, 4112 (1990).
[12] W. Becker, S. Long, and J. K. McIver, Phys. Rev. A **46**, R5334 (1992).
[13] W. Becker, S. Long, and J. K. McIver, Phys. Rev. A **50**, 1540 (1994).
[14] J. L. Krause, K. J. Schafer, and K. C. Kulander, Phys. Rev. Lett. **68**, 3535 (1992).
[15] P. B. Corkum, Phys. Rev. Lett. **71**, 1994 (1993).
[16] W. Becker *et al.,* Phys. Rev. A **56**, 645 (1997).
[17] R. W. Falcone and J. Boker, Opt. Lett. **8**, 21 (1983).
[18] T. Sekikawa *et al.,* J. Opt. Soc. Am. B **15**, 1406 (1998).
[19] D. N. Fittinghoff *et al.,* J. Opt. Soc. Am. B **12**, 1955 (1995).
[20] K. W. DeLong, D. N. Fittinghoff, and R. Trebino, IEEE J. Quantum Electron. **32**, 1253 (1996).
[21] A. L'Huillier *et al.,* Phys. Rev. A **46**, 2778 (1992).
[22] P. Balcou *et al.,* J. Phys. B **32**, 2973 (1999).
[23] M. B. Gaarde *et al.,* Phys. Rev. A **59**, 1367 (1999).
[24] P. Balcou *et al.,* Phys. Rev. A **55**, 3204 (1997).
[25] A. Saenz and P. Lambropoulos, J. Phys. B **32**, 5629 (1999).
[26] Y. Kobayashi *et al.,* Opt. Lett. **23**, 64 (1998).
[27] M. Schnürer *et al.,* Phys. Rev. Lett. **83**, 722 (1999).
[28] J. M. Schins *et al.,* J. Opt. Soc. Am. B **13**, 197 (1996).
[29] T. E. Glover *et al.,* Phys. Rev. Lett. **76**, 2468 (1996).
[30] P. M. Paul *et al.,* Science **292**, 1689 (2001).
[31] M. Drescher *et al.,* Science **291**, 1923 (2001).
[32] D. J. Kane, IEEE J. Sel. Top. Quantum Electron. **4**, 278 (1998).